IEEE Access
Multidisciplinary | Rapid Review | Open Access Journal

Received February 4, 2020, accepted February 17, 2020, date of publication February 24, 2020, date of current version March 12, 2020.

Digital Object Identifier 10.1109/ACCESS.2020.2975854

Image Segmentation Using an Active Contour Model Based on the Difference Between Local Intensity Averages and Actual Image Intensities

XIAOYING SHAN[1,4], XIAOLIANG GONG[1,3], YINGCHUN REN[5], AND ASOKE K. NANDI[1,2,3], (Fellow, IEEE)

[1]College of Electronic and Information Engineering, Tongji University, Shanghai 201804, China
[2]Department of Electronic and Computer Engineering, Brunel University London, Uxbridge UB8 3PH, U.K.
[3]Key Laboratory of Embedded System and Service Computing, Ministry of Education, Tongji University, Shanghai 201804, China
[4]Normal College, Jiaxing University, Jiaxing 314001, China
[5]College of Mathematics Physics and Information Engineering, Jiaxing University, Jiaxing 314001, China

Corresponding author: Xiaoying Shan (1510481@tongji.edu.cn)

This work was supported by the Zhejiang Provincial Natural Science Foundation of China under Grant LQ20F020027 and Grant LY18A010017.

ABSTRACT The local intensity fitting active contour models can handle inhomogeneous images, but they suffer from the shortcomings of poor performance in segmenting images with severe intensity inhomogeneity and being sensitive to initializations. To overcome these problems, we put forward a robust active contour model by introducing two adjustment coefficient functions. The energy functional of the proposed model is presented by integrating the local fitting term and two adjustment coefficient functions. The local fitting term is defined by introducing two local fitting functions that approximate the image intensities inside and outside of the contour. These two adjustment coefficient functions, which improve the segmentation performance and enhance the robustness to initialization, are constructed by utilizing the Sigmoid function as well as the difference between local intensity averages and image actual intensities. The results of the experiments on synthetic and real images demonstrate that the presented model not only is capable of handling intensity inhomogeneity better under more flexible initializations but also takes less time in comparison with other region-based models. Furthermore, these two adjustment coefficients can be employed to other local intensity fitting models to enhance the robustness to initialization and to decrease the segmentation time.

INDEX TERMS Image segmentation, active contour model, adjustment coefficient functions, intensity inhomogeneity.

I. INTRODUCTION

Active contour models, originally put forward by Kass *et al.* [1], have attracted considerable attention and found an increasingly wide utilization in image segmentation [2]–[7]. An active contour model is generally represented by an energy functional and formulated in a principled way by applying the level set methods [8], [9], which implicitly represents contour curve as the zero-level set of a higher dimensional level set function. Active contour models based on level set perform image segmentation by evolving the zero-level contour curve, and thus are able to deal with topological changes adaptively.

Active contour models are able to obtain sub-pixel accuracy of object boundaries as well as smooth and closed contour as segmentation result. In the past decades, various active contour models have been presented for image segmentation. In general, active contour models fall into two categories: edge-based models [1], [6], [8], [10]–[13] and region-based models [14]–[23]. The first kind of models commonly uses the gradient information to urge the active contour curve evolve towards the boundaries of the

The associate editor coordinating the review of this manuscript and approving it for publication was Tallha Akram.

target object. These models can effectively extract an object with strong boundaries, but they cannot detect the weak edge of an object and thus undergo weak edge leakage. Meanwhile, they are sensitive to noise and the initial contour should be located near the object, otherwise the segmentation result is dissatisfactory. Distinct from the first kind of models, region-based models make use of statistical information in global or local regions to drive contour curve to obtain desirable target boundaries. Consequently, region-based models can achieve superior results than edge-based models in segmenting images with noise and weak object boundaries.

The well-known Chan-Vese (CV) model [19] is one of the typical region-based models. This model approximates the image intensities with piecewise constant. It is for this reason that it is able to segment bimodal images but is not successful in segmenting images with intensity inhomogeneity [24], [25]. To cope with intensity inhomogeneity, a lot of local region-based models have been proposed. Li *et al.* [20] defined a region-scalable fitting (RSF) energy functional by using two fitting functions to approximate image intensities in local region. The optimum fitting functions turn out to be the local intensity averages on the two sides of the contour. Afterwards some other local intensity fitting models were proposed, such as the local image fitting (LIF) model [21], the local region-based Chan–Vese (LRCV) model [22], weighted region-scalable fitting (WRSF) model [26], and so on. The LIF model uses the weighted average of the local intensity averages to approximate image intensities. The LRCV model can be seen as an improvement of the CV model by replacing the global intensity means with local intensity averages. The WRSF model presents an improvement scheme on the LBF model. In the improvement scheme, local entropy at each pixel, which enhance the robustness of the RSF model to initialization but increases the computational cost, is exploited to measure quantitatively the variation of intensity and to redefine the energy of RSF model as a weighted energy integral with the local entropy as a weight of local energy at each point. Wang *et al*. [34] put forward an entropy weighted fitting (EWF) model by taking advantage of the Kullback–Leibler divergence [27] to measure the difference between the input image and three local fitting images, and introducing an inhomogeneity entropy descriptor as weight. The above-mentioned models based on local intensity averages can segment heterogeneous images by making use of local image intensity information. However, they still tend to fall into local minimum and thus suffer from sensitivity to initialization, even though some of them allow more flexible initial contour. In addition, they are time consuming and cannot deal with severe intensity inhomogeneity effectively.

Another strategy to deal with inhomogeneity is to perform jointly segmentation and bias field estimation. The strategy is implemented by modeling an inhomogeneous image as a piecewise constant image multiplied by a bias field, which accounts for intensity inhomogeneity and varies spatially and smoothly. Many models have been put forward based on the bias field correction [28]–[32], [36]. Li *et al*. put forward a local intensity clustering (LIC) energy functional [28] to segment images with intensity inhomogeneity and to evaluate the bias field. Huang *et al*. [31] proposed a model by designing an adaptive scale parameter and constructing a region-based pressure force function. By considering local difference matrix in a modified image model, Shan *et al*. [32] advanced a local region-based fitting [LRBF] energy functional for segmentation and bias correction of images. These models are capable of segmenting inhomogeneous images with a desirable result, but they still suffer from some drawbacks such as complicated implementation and sensitivity to the location of initial contour and are often not applicable to images with severe intensity inhomogeneity.

In this work, we put forward a robust active contour model, which can achieve a good performance in segmenting inhomogeneous images with low computational complexity and is robust to initialization. First, we define the local fitting term by using the local intensity averages inside and outside of the contour. Second, two adjustment coefficient functions, which improve the segmentation performance and enhance the robustness to initialization, are constructed by utilizing the Sigmoid function and the difference between local intensity averages and image actual intensities. Next, an energy is proposed by integrating the local fitting term and two adjustment coefficient functions. This energy is then incorporated into a variational level set formulation with a level set regularization term. Furthermore, these two adjustment coefficient functions can be employed to other local intensity fitting models to enhance the robustness to the location of initial contour and achieve a decrease in the segmentation time.

The rest of this work is structured as below. Section 2 gives a brief introduction to three active contour models and discusses the reason why the RSF model is unable to segment the image correctly when initialization is inappropriate. Section 3 details our proposed model by introducing two adjustment coefficient functions. In Section 4, experimental results are presented. Section 5 provides some discussions, followed by a brief summary of the work in Section 6.

II. RELATED WORKS AND PROBLEM ANALYSIS

A. THE CV MODEL

Chan and Vese [19] proposed an active contour model by designating two constants to approximate the image intensities of the object and background. Let $\mathrm{Im} : D \subset R^2 \to R$ be an input image defined in the image domain D. The energy functional of the CV model can be written as

$$F^{CV}(\phi, c_1, c_2) = \mu\,|T| + \lambda_1 \int_{inside(T)} |\mathrm{Im}(x) - c_1)|^2\,\mathrm{d}x + \lambda_2 \int_{outside(T)} |\mathrm{Im}(x) - c_2|^2\,\mathrm{d}x \quad (1)$$

where λ_1, λ_2, and μ are positive constants; $inside(T)$ and $outside(T)$ are the area inside and outside of the curve T; c_1 and c_2 are the global intensity averages inside and outside of the curve. Let $\phi(x) : D \to R$ be a level set function.

Using the level set methods, the curve can be represented as $T = \{x \in D | \phi(x) = 0\}$. Image segmentation can be accomplished by obtaining a closed curve T to divide the image domain D into two non-overlapping areas:

$$D_1 = inside(T) = \{x \in D | \phi(x) > 0\}$$
$$D_2 = outside(T) = \{x \in D | \phi(x) < 0\}. \quad (2)$$

The functional (24) can be rewritten in terms of the level set function $\phi(x)$ as follows:

$$F^{CV}(\phi, c_1, c_2) = \mu \int_D |\nabla H_\varepsilon(\phi(x))| \, dx + \lambda_1 \int_D |\mathrm{Im}(x) - c_1)|^2 M_1(\phi(x)) dx + \lambda_2 \int_D |\mathrm{Im}(x) - c_2|^2 M_2(\phi(x)) dx \quad (3)$$

where $M_1(\phi(x)) = H_\varepsilon(\phi(x))$ and $M_2(\phi(x)) = 1 - H_\varepsilon(\phi(x))$ are the membership functions of D_1 and D_2, and $H_\varepsilon(x)$ is a regularized Heaviside function defined by

$$H_\varepsilon(x) = \frac{1}{2}\left[1 + \frac{2}{\pi} arctan\left(\frac{x}{\varepsilon}\right)\right] \quad (4)$$

Since c_1 and c_2 are the global intensity averages inside and outside the curve, CV model can segment the image with weak edge effectively, and it is insensitive to initialization. However, it often leads to poor segmentation results for images with intensity inhomogeneity.

B. THE RSF MODEL

Li *et al*. [20] developed a region-scalable fitting model to address the problem caused by intensity inhomogeneity. The energy functional is given by:

$$F^{RSF}(\phi, u_1, u_2) = \int_D \left(\sum_{i=1}^{2} \lambda_i \int_{D_i} k(x-y) |\mathrm{Im}(x) - u_i(y)|^2 M_i(\phi(x)) dx\right) dy + \nu \int_D \frac{1}{2} (|\nabla\phi(x)| - 1)^2 dx + \mu \int_D |\nabla H(\phi(x))| \, dx \quad (5)$$

The gradient descent method is implemented to optimize the functional (5). Based on variation theory, the evolution equation of ϕ is given by

$$\frac{\partial\phi}{\partial t} = -\delta_\varepsilon(\phi)(\lambda_1 e_1 - \lambda_2 e_2) + \nu\left(\nabla^2\phi - div\left(\frac{\nabla\phi}{|\nabla\phi|}\right)\right) + \mu\delta_\varepsilon div\left(\frac{\nabla\phi}{|\nabla\phi|}\right) \quad (6)$$

where λ_1, λ_2, and μ are positive constants; e_1 and e_2 are the following functions

$$e_i = \int_D k(x-y) |\mathrm{Im}(x) - u_i(y)|^2 dy, \quad i = 1, 2. \quad (7)$$

δ_ε is the derivative of H_ε, given by

$$\delta_\varepsilon = \frac{1}{\pi} \frac{\varepsilon}{\varepsilon^2 + x^2} \quad (8)$$

The optimal $u_1(x)$ and $u_2(x)$ for minimizing the functional (5) are given by

$$u_i(x) = \frac{\int k(x-y) M_i(\phi(y)) \mathrm{Im}(y) dy}{\int k(x-y) M_i(\phi(y)) dy} \quad i = 1 \text{ and } 2. \quad (9)$$

Owing to the Gaussian kernel function $k(x - y)$ in (9), the local intensity information is obtained to direct the contour evolution, thus the RSF model is able to cope with intensity inhomogeneity. However, it is incapable of dealing with severe intensity inhomogeneity effectively and sensitive to initialization [35].

C. THE LRCV MODEL

Liu *et al*. [22] presented a local region-based Chan–Vese (LRCV) model. This model is capable of segmenting inhomogeneous image by minimizing the difference between image intensity and local intensity averages. The energy functional is written as

$$F^{LRCV}(c_1, c_2, \phi) = \lambda_1 \int_D (\mathrm{Im}(x) - c_1(x))^2 H(\phi(x)) dx + \lambda_2 \int_D (\mathrm{Im}(x) - c_2(x))^2 (1 - H(\phi(x))) dx \quad (10)$$

where λ_1 and λ_2 are positive constants; $c_1(x)$ and $c_2(x)$ are the weighted intensity averages of outer-contour and inner-contour portions in a Gaussian window centered at the point x, respectively. Therefore, $c_1(x)$ and $c_2(x)$ in LRCV model are identical with $u_1(x)$ and $u_2(x)$ in the RSF model. With the information of local intensity, LRCV model is capable of segmenting inhomogeneous images. But it still suffers from the sensitivity to initialization even though it allows more flexible initial contour when compared with the RSF model.

D. PROBLEM ANALYSIS

In the subsection, we take the RSF model as an example to discuss the reason why these local intensity fitting models, which only employ the local intensity fitting functions to direct the evolution of the contour, are unable to segment the image correctly when initialization is inappropriate.

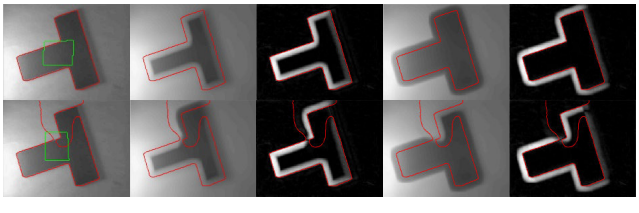

FIGURE 1. Segmentation results of LBF model. Row 1: desired result, Row 2: undesired result, Column 1: the input image with green initial contours and red final contours; Column 2-5: the images of u_1, *abs* (Im-u_1), u_2, and *abs* (Im-u_2) with red final contours, respectively.

In Fig. 1, each image contains the red final contour. Column 1 shows the segmentation results with initial contour in green. The column 2 and 4 are the image of $u_1(x)$ and

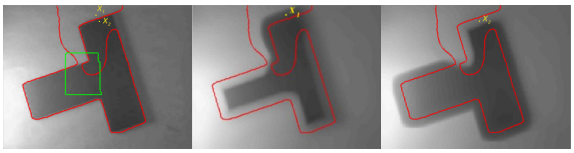

FIGURE 2. The image (a) is the leftmost image in row 2 of Fig. 1 with two points x_1 and x_2 annotated in yellow. The image (b) and (c) are the second and forth images on the left in row2 of Fig. 1 with the same two points x_1 and x_2 as image (a).

$u_2(x)$, respectively. The column 3 is the image of the absolute value of the difference between $u_1(x)$ and image intensity $\mathrm{Im}(x)$. The column 5 is the image of the absolute value of the difference between $u_2(x)$ and $\mathrm{Im}(x)$. Row 1 shows that LBF model can successfully segment the inhomogeneous image with dark object and bright background. In this situation, the value of $u_1(x)$ is larger than $\mathrm{Im}(x)$ along the interior edge, and is close to $\mathrm{Im}(x)$ along the exterior edge when the final contour lies exactly at the edge of object. Meanwhile, the value of $u_2(x)$ is smaller than $\mathrm{Im}(x)$ along the exterior edge and close to $\mathrm{Im}(x)$ along the interior edge. However, if the location of the initial curve is inappropriate, as shown in row 2, the RSF model is prone to get stuck in local optimum and thus cannot capture the target. In this situation, $u_1(x)$ and $u_2(x)$, as shown in row 2, are not the same case with row 1.

To analyze the unsatisfactory segmentation results further, we consider two points x_1 and x_2 marked in yellow in Fig. 2. The image in Fig. 2 is the leftmost image in row 2 of Fig. 1 with two points x_1 and x_2 annotated in yellow. The image (b) and (c) are obtained by marking the same points x_1 and x_2 in the second and forth images on the left in row2 of Fig. 1. Next, we analyze the unsatisfactory result in term of the value of level set function $\phi(x)$.

When the unsatisfactory results as shown in row 2 of Fig. 2 is obtained, we can see that $e_1(x_1)$ is larger than $e_2(x_1)$. This is because the difference between $u_1(y)$ and the image intensity $\mathrm{Im}(x_1)$ is bigger than the difference between $u_2(y)$ and $\mathrm{Im}(x_1)$ when the point y is in a local region centered at x_1. To achieve the minimum of the energy functional, $M_1(\phi(x_1))$ must be smaller than $M_2(\phi(x_1))$. Due to $M_2(\phi(x_1)) = 1 - M_1(\phi(x_1))$, $M(\phi(x_1))$ is smaller than 0.5 and $\phi(x_1)$ is smaller than 0. Therefore, the point x_1 is misclassified into the interior of the contour curve. Similarly, we can discuss the reason for the misclassification of x_2. Because the difference between $u_1(y)$ and $\mathrm{Im}(x_2)$ is small and the difference between $u_2(y)$ and $\mathrm{Im}(x_2)$ is relatively large when the point y is located in a local region centered at x_2, the value of $e_1(x_2)$ is smaller than $e_2(x_2)$. To reach the minimum of the energy functional, $M_1(\phi(x_2))$ must be larger than $M_2(\phi(x_2))$. This means that $M_1(\phi(x_2))$ is larger than 0.5 and $\phi(x_2)$ is bigger than 0. Therefore, the point x_2 is misclassified into the exterior of the contour curve.

1) For $x \in object$, $e_1(x)$ should be bigger than $e_2(x)$ to make it sorted into the interior of the contour.
2) For $x \in background$, $e_1(x)$ should be smaller than $e_2(x)$ to make it sorted into the exterior of the contour.

As mentioned above, the existing active contour models based on local intensity fitting functions have their limitations. To solve this problem, we construct two adjustment coefficient functions to prevent the energy functional from falling into local minimum and meanwhile deal with severe intensity inhomogeneity effectively.

III. OUR MODEL

A. LOCAL FITTING TERM

Consider a grey image $\mathrm{Im} : D \to R$, where $D \subset R^2$ is the image domain. For a given point $x \in D$, D_x is a neighborhood centered at x. The local fitting term (LFT) at x is defined as:

$$LFT(x) = \int_{D_x} |\mathrm{Im}(x) - u(y)|^2 \, \mathrm{d}y, \tag{11}$$

where $u(y)$ represents the local intensity average and it is defined within a local region as explained in following paragraph. In the proposed energy functional, a truncated Gaussian function $k(x-y)$, such that $k(x-y) = 0$ for $y \notin D_x$, is introduced as a nonnegative window function. The truncated Gaussian function $k(x-y)$ is defined by

$$k(u) = \begin{cases} \frac{1}{a} e^{-|u|^2/2\sigma^2}, & for \ |u| \le \rho \\ 0, & \text{otherwise} \end{cases} \tag{12}$$

where ρ is the radius of the neighborhood, σ is the standard deviation of the Gaussian function, and a is a normalization constant such that $\int k(u) = 1$. With the function $k(x-y)$, $LFT(x)$ in (11) can be rewritten as

$$LFT(x) = \int_D k(x-y) \, |\mathrm{Im}(x) - u(y)|^2 \, \mathrm{d}y \tag{13}$$

Considering the Gaussian function $k(x-y)$, the local intensity averages inside and outside of the contour T, $u_1(y)$ and $u_2(y)$ are defined as

$$\begin{aligned} u_1(y) &= \frac{\int k(x-y) M_1(\phi(x)) \mathrm{Im}(x) dx}{\int k(x-y) M_1(\phi(x)) dx} \\ u_2(y) &= \frac{\int k(x-y) M_2(\phi(x)) \mathrm{Im}(x) dx}{\int k(x-y) M_2(\phi(x)) dx} \end{aligned} \tag{14}$$

B. THE ADJUSTMENT COEFFICIENT FUNCTIONS

The Sigmoid function and the difference between local intensity averages and actual image intensities are utilized to construct two adjustment coefficient functions $S(u_1(x) - \mathrm{Im}(x))$ and $S(\mathrm{Im}(x) - u_2(x))$ where $u_1(x)$ and $u_2(x)$ can be calculated by (14) and S is Sigmoid function defined by

$$S(z) = \frac{1}{1 + e^{-z}}. \tag{15}$$

Obviously, the value range of $S(z)$ is (0, 1) and

$$S(z) \approx \begin{cases} 1, & z \gg 0 \\ 0, & z \ll 0 \\ 0.5, & z \approx 0. \end{cases} \tag{16}$$

C. THE ENERGY FUNCTIONAL BASED ON TWO ADJUSTMENT COEFFICIENT FUNCTIONS

Using the adjustment coefficient functions, we now present a robust local region-based model for image segmentation. The proposed model incorporates local intensity statistical information and the difference between local intensity means and actual image intensities into its energy functional, defined as:

$$E(u_1, u_2, T) = \mu\,|T| + \int_{inside(T)} \lambda_1 m_1(x)dx + \int_{outside(T)} \lambda_2 m_2(x)dx \quad (17)$$

where λ_1, λ_2, and μ are positive constants; $|T|$ represents the length of the contour T and thus makes sure the length can reach the optimal value in segmentation result, m_1 and m_2 are given by:

$$\begin{aligned} m_1(x) &= S(u_1(x)-\mathrm{Im}(x)) \int_D k(x-y)\,|\mathrm{Im}(x)-u_1(y)|^2 dy \\ m_2(x) &= S(\mathrm{Im}(x)-u_2(x)) \int_D k(x-y)\,|\mathrm{Im}(x)-u_2(y)|^2 dy \end{aligned} \quad (18)$$

Using level set methods, we rewrite the energy functional (17) as

$$\begin{aligned} E(u_1, u_2, \phi) = \mu \int_D |\nabla H(\phi(x))|\,\mathrm{d}x \\ + \int_D \lambda_1 m_1(x) M_1(\phi(x))dx \\ + \int_D \lambda_2 m_2(x) M_2(\phi(x))dx \end{aligned} \quad (19)$$

To maintain the level set function ϕ close to a signed distance function during the contour evolution, $\Re(\phi) = \int_D \frac{1}{2}(|\nabla\phi(x)| - 1)^2\,\mathrm{d}x$ called the distance regularization term is incorporated into the energy functional (19). Thus, total energy functional of the proposed model is expressed as

$$\begin{aligned} E(u_1, u_2, \phi) = \nu \int_D \frac{1}{2}(|\nabla\phi| - 1)^2 dx + \mu \int_D |\nabla H(\phi(x))|\,\mathrm{d}x \\ + \int_D \lambda_1 m_1(x) M_1(\phi(x))dx \\ + \int_D \lambda_2 m_2(x) M_2(\phi(x))dx \end{aligned} \quad (20)$$

D. ENERGY FUNCTIONAL MINIMIZATION

We minimize the energy functional (20) by using the gradient descent method. For a fixed level set function $\phi(x)$, the functional $E(u_1, u_2, \phi)$ is optimized with respect to $u_1(x)$ and $u_2(x)$, which can be calculated by (14). Keeping $u_1(x)$ and $u_2(x)$ fixed, we minimize the functional (20) with respect to $\phi(x)$ by solving the following gradient flow equation

$$\begin{aligned} \frac{\partial\phi}{\partial \mathrm{t}} &= -\delta_\varepsilon(\phi)(\lambda_1 m_1 - \lambda_2 m_2) \\ &\quad + \upsilon\left(\nabla^2\phi - div\left(\frac{\nabla\phi}{|\nabla\phi|}\right)\right) + \mu\delta_\varepsilon(\phi) div\left(\frac{\nabla\phi}{|\nabla\phi|}\right) \end{aligned} \quad (21)$$

The initial level set function $\phi(x)$ is initialized as

$$\phi(x) = \begin{cases} -c_0 & x \text{ is inside } D_0, \\ c_0 & x \text{ is outside } D_0, \end{cases} \quad (22)$$

It is noteworthy that when the input images have bright background and dark objects of interest, c_0 equals 2. However, if the input images have dark background and bright objects of interest, we set c_0 to be -2. In order to measure computing time, we apply $|(A_{i+5} - A_i)/A_i| < 10^{-5}$ as the stopping criterion of curve evolution. A_i stands for the region inside the contour curve at the iteration i. Algorithm 1 summarizes the procedure for the proposed model.

Algorithm 1

1: **Set parameters including** c_0.
2: **Input the image** $Im(x)$ **and initialize the level set function** ϕ_0.
3: **For** $t \leftarrow 1$ **to iteration do.**
4: **Compute** $u_1(x)$ **and** $u_2(x)$ **according to (14).**
5: **Calculate** m_1 **and** m_2 **according to (18).**
6: **Update the level set function according to (21).**
7: **if** $|(A_{i+5} - A_i)/A_i| < 10^{-5}$ **or the fixed iterative times is reached, then end.**
8: **Output the segmentation result** $\phi = \phi_{i+1}$.

IV. EXPERIMENTAL RESULTS

In this section, a lot of experiments are conducted to test our proposed model with synthetic and real images. All the experiments have been performed with MATLAB 2011b on a laptop with Intel Core i7-8565U CPU 1.80 GHz and RAM 16.0GB. Unless indicated otherwise, we utilize the following parameters in all the experiments: $\lambda_1 = \lambda_2 = 1$, $\Delta t = 0.1$, $\nu = 1$, $\mu = 0.004 \times 255^2$, and parameter of Gaussian kernel $\sigma = 3.0$. We compare our model with CV [19], RSF [20], WRSF [26], LRCV [22], LIC [28], LRBF [32], and EWF [34].

A. SEGMENTATION RESULTS OF OUR MODEL

Fig. 3 shows the segmentation processes of our model in segmenting four images. The first two images exhibit intensity inhomogeneity, the second and third images are contaminated by noise and the last one has irregular texture. For the image in row 4 of Fig. 1, μ is set to be 0.04*255*255 and σ is 5 in our model. The column 1 are images with initial contours. Column 2 to 4 are the contour evolution processes of our model. Column 5 are the images with the final contours. It is noteworthy that column 2 shows the contour after one iteration. From column 2, we can see that the new contours emerge at the boundaries of the object soon just after one iteration in our model due to these adjustment coefficient functions $S(u_1(x) - \mathrm{Im}(x))$ and $S(\mathrm{Im}(x) - u_2(x))$. These experiments verify that our model is capable of achieving satisfactory segmentation results for image with intensity inhomogeneity and noise.

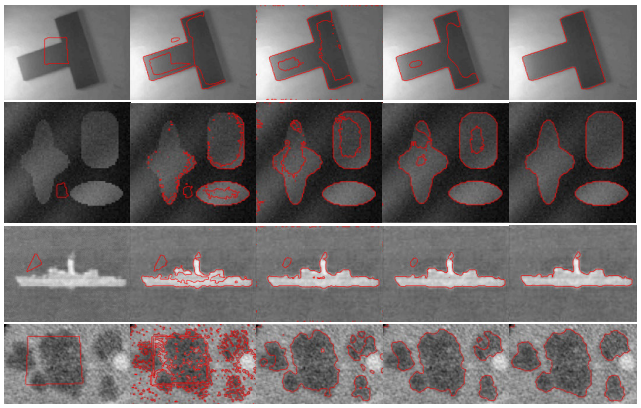

FIGURE 3. Segmentation processes of our model. Column 1: images with initial contours. Column 2 to 4: evolution process. Column 5: the final contours.

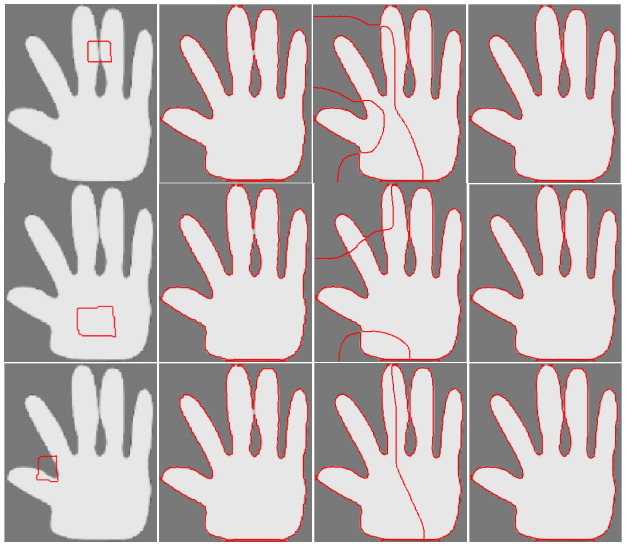

FIGURE 4. Comparison results of our model with CV and LBF in segmenting a hand image which is a bimodal image. Column 1: images with red initial contours, column 2 – 4: the results with final contours from CV, LBF and our model, respectively.

B. BIMODAL IMAGE SEGMENTATION

Fig. 4 and 5 show the comparison of our model with CV and LBF in segmenting bimodal images. Two test images in these experiments are a hand image and a synthetic image. Column 1 shows images with initial contours and the results from CV, LBF and the proposed model are displayed in column 2 to 4. It is well known that the CV model can segment bimodal image successfully and it is more robust to initialization than local region-based model such as LBF. Therefore, our model is compared with CV model in segmenting bimodal images. As shown in Fig. 4 to 5, CV and our model have obtained similar results for the synthetic image by visual comparison. However, for the hand image in which the middle finger and ring finger stick together, CV model fails to get desired segmentation accuracy of the finger boundaries, but the eventual contour of our model can reflect the authentic

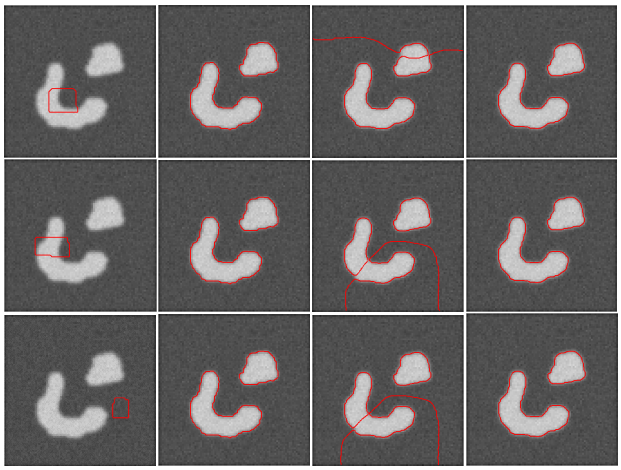

FIGURE 5. Comparison results of our model with CV and LBF in segmenting a synthetic bimodal image. Column 1: images with red initial contours, column 2 – 4: the results with final contours from CV, LBF and our model, respectively.

hand shape precisely. Evidently, LBF model fails to segment them with the given initial contours due to its sensitivity to initialization. It can be observed that our model can efficiently segment bimodal images and is robust to the initial contour.

C. INHOMOGENEOUS IMAGE SEGMENTATION

Fig. 6 to 9 show comparison results of our proposed model with CV, LBF, WRSF, LRCV, LIC, LRBF, and EWF in segmenting images with intensity inhomogeneity. μ is set to be 0.0035×255^2 and 0.0055×255^2 in our model for the images in Fig. 8 and 9, respectively. σ in our model is 5 for images in Fig. 9. In Fig. 6 to 9, the images with initial contours are displayed in the first column, the results from CV, LBF, WRSF, LRCV, LIC, LRBF, EWF and our model in column 2 to 9. Four test images and four different initializations for each image are used in these experiments. As shown in Fig. 6 to 9, CV model cannot handle intensity inhomogeneity and the LBF, WRSF, LRCV, LIC, LRBF, and EWF models can obtain satisfactory results only under some initial contours. However, our model is capable of achieving the desired segmentation for each initialization. The experiments establish that our model is robust to the location of initial contour.

We also quantitatively evaluated the performance of these models in term of Dice Similarity Coefficient (DSC) [6], [33] defined by:

$$DSC = \frac{2N(G \cap T)}{N(G) + N(T)} \tag{23}$$

where N ($\bullet$) presents the number of pixels; $\cap$ is the intersection operator; T is the result of a test model; G is the ground truth obtained by the manual segmentation. The value of DSC varies between 0 and 1, and the larger the value, the more accurate is the result of the model. For convenience, we label the image in Fig. 6 to 9 as image A to D in sequence. The segmentation accuracies are listed in Table 1 based on

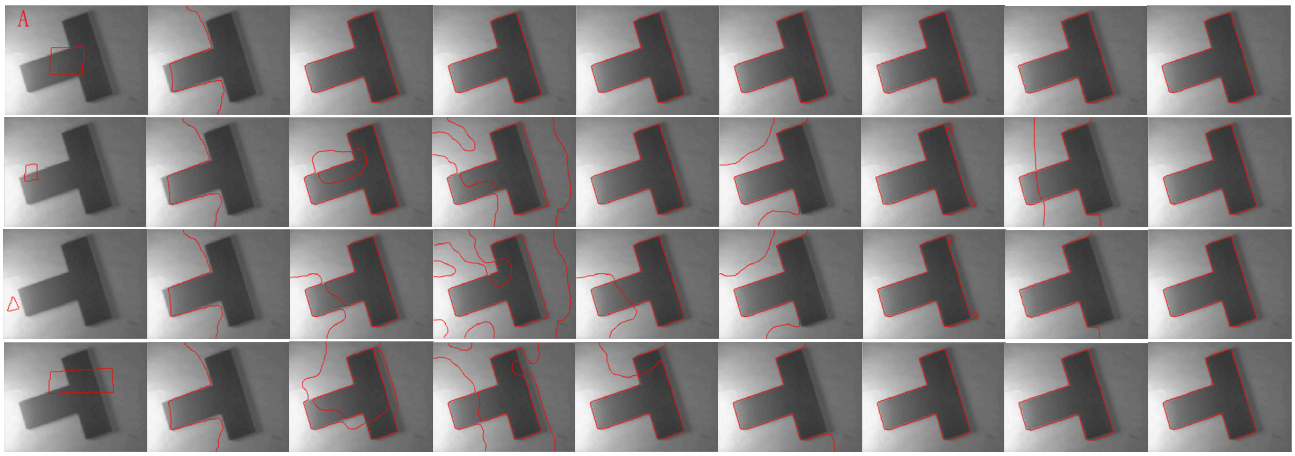

FIGURE 6. Comparison results of our model with CV, LBF, WRSF, LRCV, LIC, LRBF, and EWF on a real inhomogeneous image of a T-shape object. Column 1: images with initial contours, column 2 – 9: the results from CV, LBF, WRSF, LRCV, LIC, LRBF, EWF, and our model.

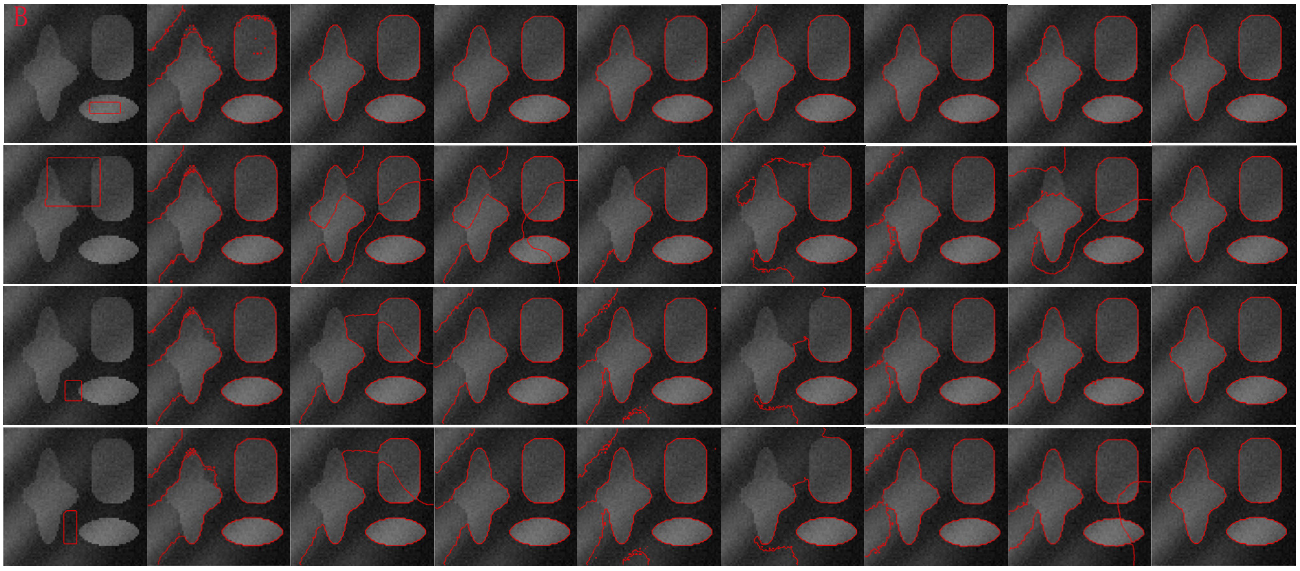

FIGURE 7. Comparison results of our model with CV, LBF, WRSF, LRCV, LIC, LRBF, and EWF on a synthetic image with intensity inhomogeneity. Column 1: images with initial contours, column 2 – 9: the results from CV, LBF, WRSF, LRCV, LIC, LRBF, EWF, and our model.

image A to D. It should be noted that we only list the segmentation accuracy under the first initialization for each image. This is because only under these initial contours, all of the test models can obtain satisfactory segmentation results.

Additionally, the CPU time and the iteration times of these models in the experiments are recorded in Table 2. As shown in Table 1 and 2, the CV model is very fast, but it does not perform well in dealing with intensity inhomogeneity because of utilization of global intensity means for classification. The EWF model can get desirable segmentation results but it is the most time consuming. Three different local fitted images are utilized in the EWF model to achieve reasonable segmentation accuracy, but they make the model time-consuming in the process. The LIC model is not successful in segmenting inhomogeneous images except the first image. Even LBF, WLBF, LRCV, LRBF, and EWF can extract objects of the interest, they consume more time than our model. The comparison of these models shows that our model not only can achieve better results in segmenting images with intensity inhomogeneity, but also can perform segmentation in less CPU time and iterations.

In order to test further the robustness of our model to contour initializations, we apply our model to these four images (Fig. 6 to 9) with 20 different initializations for each image to test quantitatively the capability of our model. Four of 20 different initializations are shown in Fig. 6 to 9. The segmentation accuracies for 20 different initializations are shown in Fig.10. As shown in Fig. 10, the segmentation accuracy from our model is very stable. For image D, although the segmentation accuracy from our model varies slightly with the initialization, the segmentation accuracy almost ranges between 0.975 and 0.985. These experiments

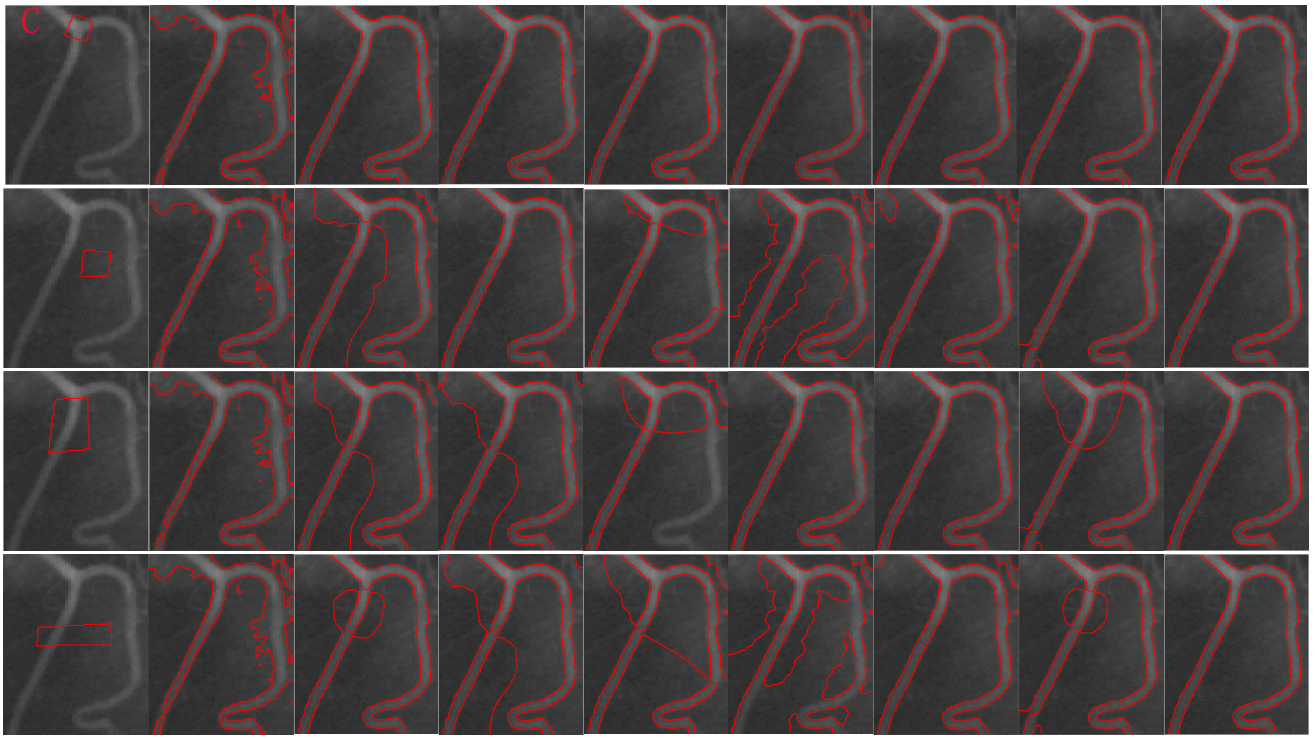

FIGURE 8. Comparison results of our model with CV, LBF, WRSF, LRCV, LIC, LRBF, and EWF on a X-ray image of vessels. Column 1: images with initial contours, column 2 – 9: the results from CV, LBF, WRSF, LRCV, LIC, LRBF, EWF, and our model.

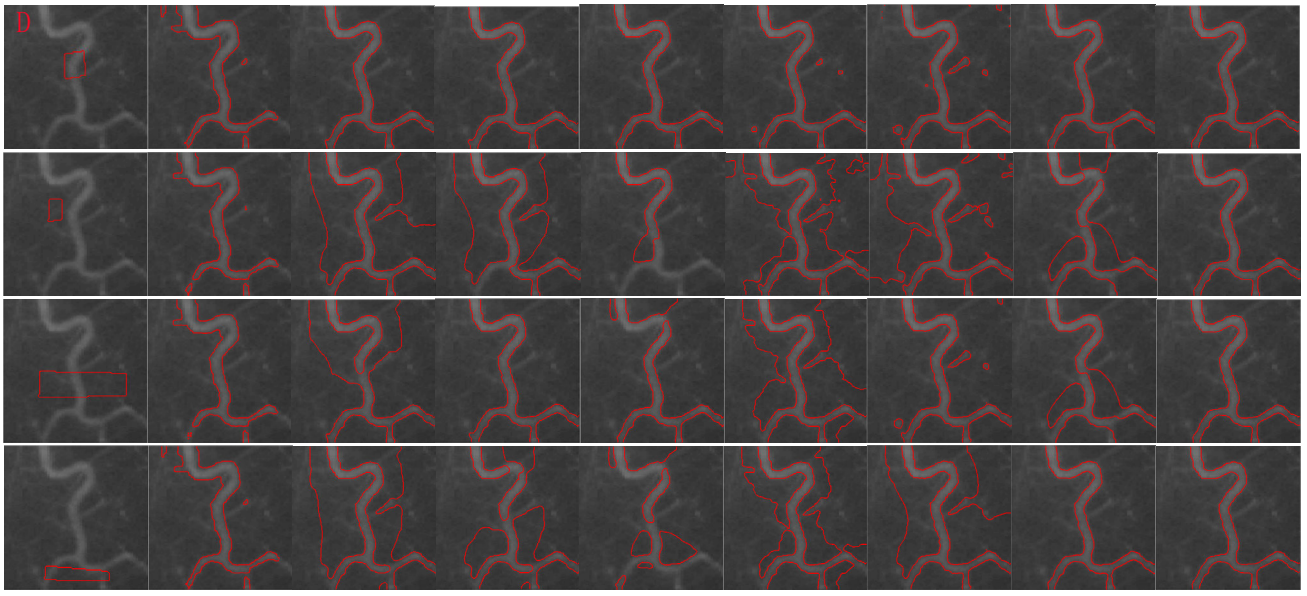

FIGURE 9. Comparison results of our model with CV, LBF, WRSF, LRCV, LIC, LRBF, and EWF on a X-ray image of vessels. Column 1: images with initial contours, column 2 – 9: the results from CV, LBF, WRSF, LRCV, LIC, LRBF, EWF, and our model.

verify the robustness of our model to initial contour as well as a desirable accuracy. We have demonstrated that our proposed model is better than all these models, including LBRF model and EWF model.

In this experiment, we use five images in Fig.11 to verify further the superiority of our model. The value of μ is set to 0.001×255^2, 0.04×255^2, 0.007×255^2, 0.015×255^2 and 0.1×255^2 in our model for the images in Fig. 11. The value of σ in our model is 8 and 12 for images in row 3 and 4, respectively. We compare our model with LBF, WRSF, LRCV, LIC, LRBF, and EWF on these images including a synthetic image, a real flower image, a magnetic resonance (MR) brain image,

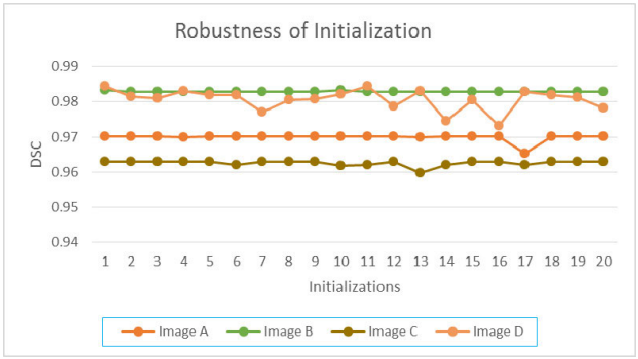

FIGURE 10. Curves of the segmentation accuracy of our model under 20 different initial contours for each image shown in Fig. 6 to 9.

a CT image of heart and an ultrasound image of left ventricle. All of the images in Fig. 11 exhibit intensity inhomogeneity. The ultrasound image of left ventricle is corrupted by noisy as well as intensity inhomogeneity. Desirable parameters and initializations are set for LBF, WRSF, LRCV LIC, LRBF, and EWF. For the synthetic image, LBF, WRSF, and LIC cannot achieve satisfactory results. Even though the WRSF model uses local entropy to measure quantitatively the variation of image intensity, it still fails to segment the images in row 1. The LIC model is built up based on modeling an inhomogeneous image as a piecewise constant image multiplied by a bias field, however it is incapable of segmenting images with serve intensity inhomogeneity such as the images in row 1, 2 and 5. The LRBF model can get desirable results for the images in row 1, 4 and 5, but is not competent for the images in row 2 and 3. Even though EWF takes into account of inhomogeneity entropy, it is not able to locate target objects from inhomogeneity regions for the image in row 4. As shown in Fig. 11, it is obvious that our model is able to extract the object boundaries more precisely than the other models in segmenting images contaminated by noises and intensity inhomogeneity.

We compared quantitatively our model with LBF, WRSF, LRCV, LIC, LRBF, and EWF based on 19 natural images randomly chosen from the BSDS500 dataset [37]. Fig. 12 shows some segmentation results of the experiments. The ground truth of these images obtained from BSD500 dataset are shown in row 1. The value of μ in our model is set to 0.15*255*255 for the images in column 2 to 4 while the value of σ is set to 7 for image in column 3. Desirable parameters and initializations are set for LBF, WRSF, LRCV, LIC, LRBF, and EWF. We can see all the model can handle the image in row 1 and get similar results. Our model and EWF can get similar desirable segmentation results for the image in column 4. For the plane image, only our model, LRCV and EWF can achieve satisfactory results and apparently our model achieves better result. As for the images in column 3, our model also outperforms the other models. The DSC values of these seven models based on the 19 natural images are displayed in Fig.13. Mean values of DSC of LBF, WRSF, LRCV, LIC, LRBF, EWF, and our model are 0.881, 0.882, 0.884, 0.784, 0.875, 0.895, and 0.918 with the standard deviations of 0.057, 0.062, 0.058, 0.153, 0.084, 0.059, and 0.050. These experiments demonstrate that the proposed model has better segmentation performance compared with the other models, and is able to separate the objects of interest from the heterogeneous and complex background.

V. DISCUSSION

A. INITIALIZATION OF LEVEL SET FUNCTION

When the input images have bright background and dark objects of interest, c_0 is set to be 2 in our model. If the input images have dark background and bright objects of interest,

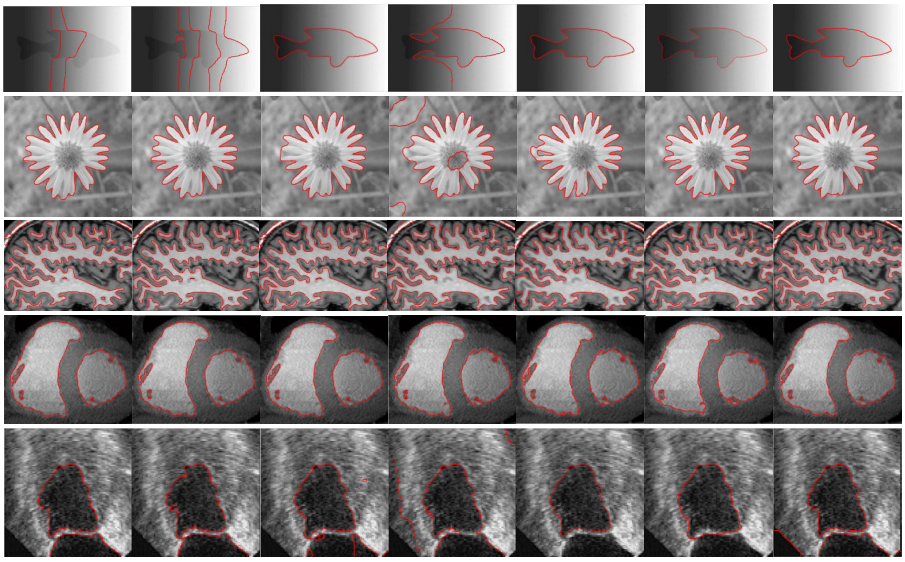

FIGURE 11. Comparison results of our model with LBF, WRSF, LRCV, LIC, LRBF, EWF, and our model for inhomogeneous images. Column 1 – 7: the results from LBF, WRSF, LRCV, LIC, LRBF, EWF, and our model.

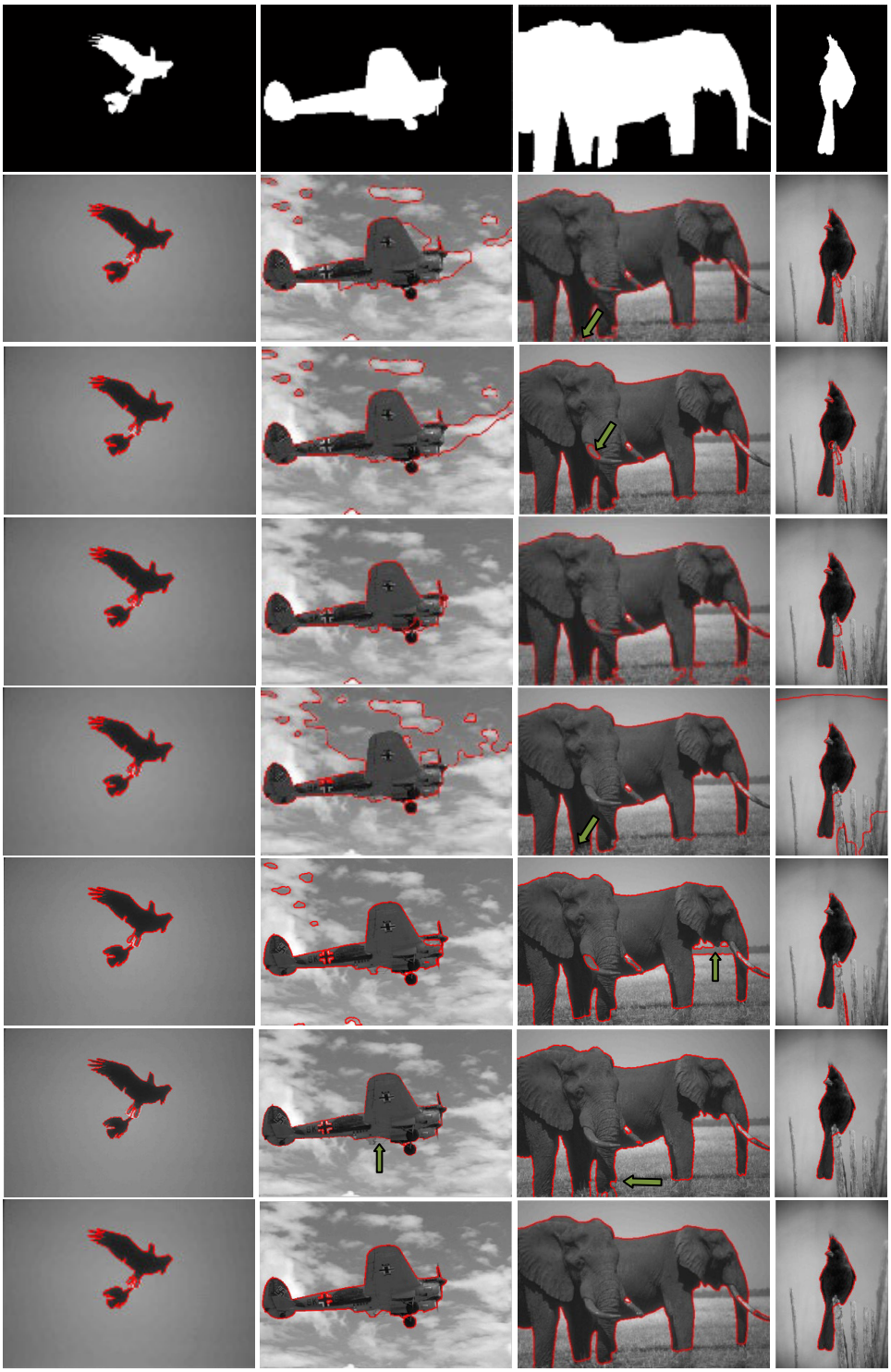

FIGURE 12. Comparison results of our model with LBF, WRSF, LRCV, LIC, LRBF, and EWF for natural images from BSD500 dataset. Row1: the ground truth, row 2– 8: the results from LBF, WRSF, LRCV, LIC, LRBF, EWF, and our model.

c_0 is set to be -2. Next, we take two images shown in Fig. 14 as examples to illustrate the need for such initialization.

Fig. 14 shows the comparison of the results which are gained by applying our model to two images and by setting c_0 to be 2 and -2 for each image. One of these images is an image with bright background and dark object of interest, the other one with bright object of interest and dark background. No matter which image, we can see that the images of u_1 and u_2 obtained by two different initializations are similar; however, the final contour curves are distinct

TABLE 1. Comparison of segmentation accuracy in term of DSC. The largest value of DSC for each image is in green (best), the second biggest in blue (second best), and smallest in red (worst).

Mode ls / Images	CV	LBF	WRSF	LRCV	LIC	LRBF	EWF	Our model
Image A	0.523	0.970	0.969	0.972	0.968	0.967	0.971	0.970
Image B	0.816	0.983	0.983	0.981	0.835	0.982	0.981	0.983
Image C	0.720	0.962	0.959	0.961	0.937	0.961	0.960	0.963
Image D	0.819	0.976	0.977	0.966	0.908	0.974	0.983	0.984
mean	0.720	0.973	0.972	0.970	0.912	0.971	0.974	0.975

TABLE 2. CPU time and number of iterations of eight methods for the images shown in Fig. 6 to 9. The smallest value of CPU time for each image is in green (best), the second smallest in blue (second best), and largest in red (worst).

Models / Images (size)	CV	LBF	WRSF	LRCV	LIC	LRBF	EWF	Our model
	Iterations Time(s)	Iterations/ Time(s)	Iterations/ Time(s)	Iterations/ Time(s)	Iterations/ Time(s)	Iterations / Time (s)	Iterations / Time (s)	Iterations/ Time(s)
Image A(96*127)	75/0.22	85/0.95	65/0.78	160/1.46	515/5.41	65 / 1.72	360/4.68	50/0.31
Image B(75*79)	45/0.07	165/0.95	135/0.97	225/1.13	140/0.77	95 / 0.86	160/ 2.14	40/0.27
Image C(131*103)	165/0.41	225/2.42	240/2.73	420/3.95	70/1.11	106 / 3.30	80/1.41	45/0.58
Image D(110*111)	80/0.20	145/1.67	130/1.13	220/1.83	180/2.13	110 / 2.19	120/2.16	35/0.89
Mean of time (s)	0.23	1.50	1.40	2.09	2.36	2.02	2.60	0.51

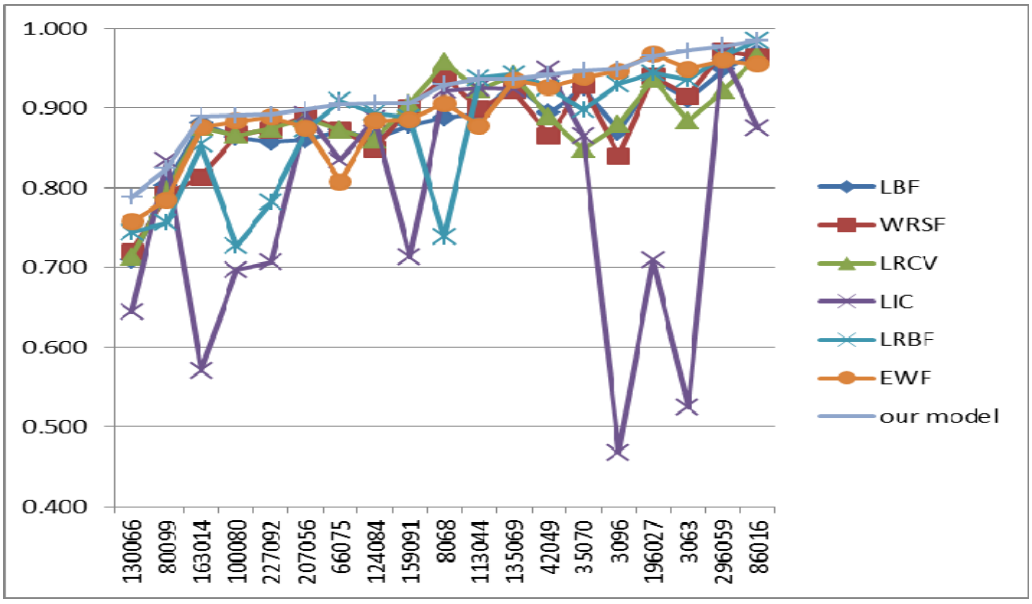

FIGURE 13. Comparison results of our model with LBF, WRSF, LRCV, LIC, LRBF, and EWF in terms of DSC for 19 randomly chosen images from BSDS500 dataset.

from one another. As shown in the column 2 of Fig. 14, new zero-level contours emerge near the inner boundaries of the object, when c_0 is set to be -2 for the first image and 2 for the second image. The term $\mathcal{L}(\phi)$ is able to make the length of the zero-level contour inside the object smaller and smaller, and disappear eventually. Thus, our model can get desirable final contour. But if c_0 is set to be 2 for the first image and -2 for the second image., the new zero-level contours emerge near the outer boundaries of the object. In this situation, the length regularization term $\mathcal{L}(\phi)$ cannot make the zero-level contours outside the object disappear. Therefore, c_0 is set to be 2 for the images with bright background and dark objects of interest, and -2 for the images with dark background and bright objects of interest.

B. FUNCTION OF TWO ADJUSTMENT COEFFICIENT FUNCTIONS

In this subsection, we explain how these two adjustment functions guarantee the robustness of the proposed model.

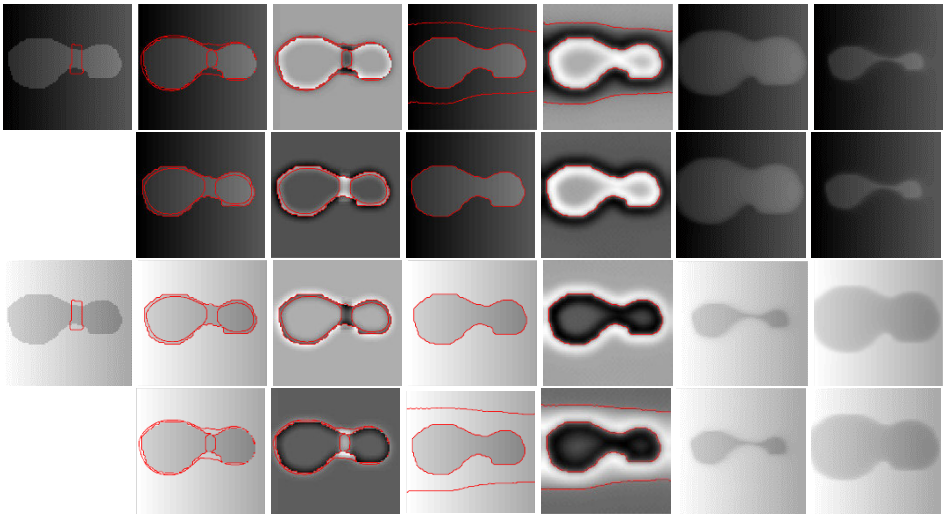

FIGURE 14. The segmentation results from our model by setting c_0 to be 2 and −2. The results in row1 and row3 are obtained by setting c_0 to be 2. The results in row2 and row4 are obtained by setting c_0 to be −2. Column1: the input image with the initial contour. Column2 to 3: the input images and images of $\phi(x)\phi(x)\phi(x)$ with zero- level contour after 1 iteration. Column4 to 5: the input images and images of $\phi(x)\phi(x)\phi(x)$ with final zero- level contour. Column6 to7 are the u1 and u2 images of final segmentation results.

For convenience, we list the functions $m_1(x)$ and $m_2(x)$ in (21):

$$\begin{aligned} m_1(x) &= S(u_1(x) - \mathrm{Im}(x)) \int_D k(x-y)\,|\mathrm{Im}(x) - u_1(y)|^2 dy \\ &= S(u_1(x) - \mathrm{Im}(x))e_1(x) \\ m_2(x) &= S(\mathrm{Im}(x) - u_2(x)) \int_D k(x-y)\,|\mathrm{Im}(x) - u_2(y)|^2 dy \\ &= S(\mathrm{Im}(x) - u_2(x))e_2(x) \end{aligned} \tag{24}$$

where $e_1(x)$ and $e_2(x)$ are the functions in (7). To illustrate the function of these two adjustment coefficient functions, the initial level set function of our model is set in a special way in the experiment.

We take an undesirable result from LBF model as the initialization of our model. The images in row 1 of Fig. 15 are the same images in Fig. 2. The red contour is the final contour from LBF model when it has the green contour as the initialization. In this case, LBF model is stuck in local minimum. We set the final level set function from LBF model, which corresponds to the red final contour, to be the initial level set function in our model. Therefore, at the beginning of image segmentation in our model, $e_1(x_1)$ is larger than $e_2(x_1)$ and $S(u_1(x_1)-\mathrm{Im}(x_1))$ is smaller than $S(\mathrm{Im}(x_1)-u_2(x_1))$. The segmentation process of our model is shown in row 2 of Fig. 15. To achieve minimum, $M_1(\phi(x_1))$ tends to be larger and larger, and $M_2(\phi(x_1))$=1 − $M_1(\phi(x_1))$ tends to be smaller and smaller. This leads to the evolution of the level set function $\phi(x)$. Along with the evolution, $u_1(x_1)$ is getting larger and $u_2(x_1)$ smaller. Consequently, $e_1(x_1)$ is getting smaller and smaller, and $e_2(x_1)$ larger and larger. Meanwhile, $S(u_1(x_1) - \mathrm{Im}(x_1))$ is getting larger and $S(\mathrm{Im}(x_1) - u_2(x_1))$ smaller until the contour is located at the boundary of the object. At this point, $S(u_1(x_1) - \mathrm{Im}(x_1)) < S(\mathrm{Im}(x_1) - u_2(x_1))$ and $e_1(x_1) < e_2(x_1)$, so the value of $\phi(x_1)$ tend to be stable. For the point x_2, $e_1(x_2)$ is smaller than $e_2(x_2)$, and $S(u_1(x_2) - \mathrm{Im}(x_2))$ is larger than $S(\mathrm{Im}(x_2) - u_2(x_2))$ in the beginning. To achieve minimum, $M_1(\phi(x_2))$ tend to be smaller and smaller, and $M_2(\phi(x_2))$ larger and larger. This results in the evolution of the level set function $\phi(x)$. Along with the evolution of $\phi(x)$, $e_1(x_2)$ is getting larger and larger, and $e_2(x_2)$ smaller and smaller. Meanwhile, $S(u_1(x_2) - \mathrm{Im}(x_2))$ is getting smaller and $S(\mathrm{Im}(x_2) - u_2(x_2))$ larger until the contour is located at the boundary of the object. At this moment, $S(u_1(x_2) - \mathrm{Im}(x_2)) > S(\mathrm{Im}(x_2) - u_2(x_2))$ and $e_1(x_2) > e_2(x_2)$, so the value of $\phi(x_2)$ tend to be stable.

From the above experiments and analysis, we can see that these two adjustment coefficient functions can stop the energy functional of our model from being stuck in local minimum, and drive the contour curve towards the boundary of the object.

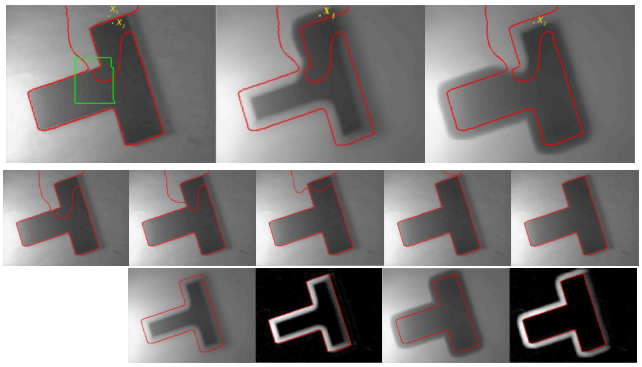

FIGURE 15. The images in row 1, which are the same images in Fig. 2, are the segmentation results from LBF model. They are the input image with green initial contours and red final contours, the images of u1 and u2, respectively. Row 2 is the segmentation process of our model with the red final contour in row 1 as the initialization. Row 3 shows the segmentation results from our model, which are the images of u_1, *abs* (*Im* - u_1), u_2, and *abs* (*Im*-u_2) with red final contours, respectively.

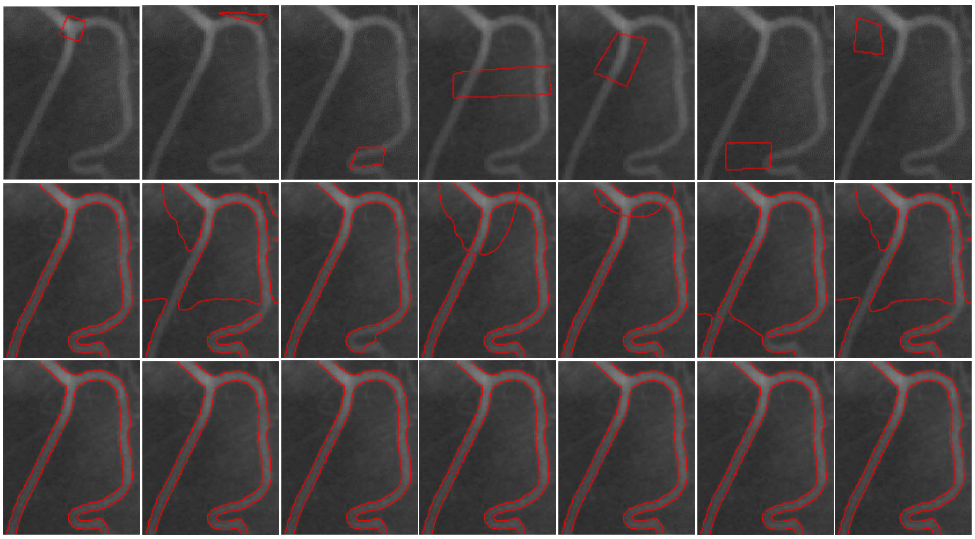

FIGURE 16. Comparison results of LRCV and improved LRCV model. Row 1: images with initial contours, row 2-3: the results of LRCV and improved LRCV, respectively.

C. APPLICATION EXTENSION OF THESE TWO ADJUSTMENT COEFFICIENT FUNCTIONS

In the proposed model, we use the difference between local average intensities and actual image intensities to define two adjustment coefficient functions to drive the evolution of the level set function in right direction. In other word, the difference between the RSF energy and the improved energy is that the improved energy has two adjustment coefficient functions. In fact, these two adjustment coefficient functions can be employed in other local intensity fitting models, such as the LRCV, to enhance the robustness to initial contour and improve the speed of segmentation.

By using these two adjustment coefficient functions to redefine the energy of LRCV model to be a weighted integral and integrating $\Re(\phi)$ and the term $|T|$ represents the length of the contour T, the entire energy functional of the meliorated LRCV model is written as

$$\begin{aligned} &E(u_1, u_2, \phi) \\ &= \mu \int_D \frac{1}{2} (|\nabla\phi(x)| - 1)^2 \, dx + \nu \int_D |\nabla H(\phi(x))| \, dx \\ &\quad + \lambda_1 \int_D (\mathrm{Im}(x) - u_1(x))^2 S(u_1(x) - \mathrm{Im}(x)) H(\phi(x)) dx \\ &\quad + \lambda_2 \int_D (\mathrm{Im}(x) - u_2(x))^2 \, S(\mathrm{Im}(x) - u_2(x)) \\ &\quad \times (1 - H(\phi(x))) \, dx \end{aligned} \tag{25}$$

Fig. 16 shows comparison results of the improved LRCV with LRCV. The LRCV model can segment the image of vessel correctly when the initial contour is appropriate. However, it suffers from the sensitivity to initialization. By using these two adjustment coefficient functions to evolve the contour in right direction, the improved LRCV model can achieve desired segmentation results under each initial contour. In addition, the iteration number of LRCV model is 420 and the CPU time is 3.95 seconds. The iteration number of the improved LRCV model is only 85 and the CPU time is 0.95 seconds. These experiments establish that these two adjustment coefficient functions can be employed in other local intensity fitting models to improve computational efficiency and to enhance the robustness to initialization.

D. APPLICATION SCOPE OF THE PROPOSED MODEL

The proposed model is applicable for two-phase segmentation of images in which the object is brighter than background or the object is darker than background. However, it cannot segment successfully when parts of the object are brighter and other parts of the object are lighter than the background, as the image shown in Fig. 17.

FIGURE 17. Undesirable segmentation result for a nature image in the proposed model.

VI. CONCLUSION

In this work, we have put forward a local intensity fitting active contour model by introducing two adjustment coefficient functions. These two adjustment coefficient functions, which improve the segmentation performance and enhance the robustness to initialization, are constructed by utilizing the Sigmoid function and the difference between local average intensities and image actual intensities. Results from

systematic experiments demonstrate that the proposed model is not only robust to initializations but also achieves better performance in terms of accuracy and efficiency when compared with other region-based models. In addition, these two adjustment coefficient functions can be employed in other local intensity fitting models to accelerate the evolution of curve towards the boundaries of object and enhance the robustness to initialization.

REFERENCES

[1] M. Kass, A. Witkin, and D. Terzopoulos, "Snakes: Active contour models," *Int. J. Comput. Vis.*, vol. 1, no. 4, pp. 321–331, Jan. 1988.

[2] N. Paragios and R. Deriche, "Geodesic active contours and level sets for the detection and tracking of moving objects," *IEEE Trans. Pattern Anal. Mach. Intell.*, vol. 22, no. 3, pp. 266–280, Mar. 2000.

[3] M. Gong, H. Li, X. Zhang, Q. Zhao, and B. Wang, "Nonparametric statistical active contour based on inclusion degree of fuzzy sets," *IEEE Trans. Fuzzy Syst.*, vol. 24, no. 5, pp. 1176–1192, Oct. 2016.

[4] Y. Zhou, W.-R. Shi, W. Chen, Y.-L. Chen, Y. Li, L.-W. Tan, and D.-Q. Chen, "Active contours driven by localizing region and edge-based intensity fitting energy with application to segmentation of the left ventricle in cardiac CT images," *Neurocomputing*, vol. 156, pp. 199–210, May 2015.

[5] G. Kasinathan, S. Jayakumar, A. H. Gandomi, M. Ramachandran, S. J. Fong, and R. Patan, "Automated 3-D lung tumor detection and classification by an active contour model and CNN classifier," *Expert Syst. Appl.*, vol. 134, pp. 112–119, Nov. 2019.

[6] A. Khadidos, V. Sanchez, and C.-T. Li, "Weighted level set evolution based on local edge features for medical image segmentation," *IEEE Trans. Image Process.*, vol. 26, no. 4, pp. 1979–1991, Apr. 2017.

[7] S. Luo, L. Tong, and Y. Chen, "A multi-region segmentation method for SAR images based on the multi-texture model with level sets," *IEEE Trans. Image Process.*, vol. 27, no. 5, pp. 2560–2574, May 2018.

[8] V. Caselles, R. Kimmel, and G. Sapiro, "Geodesic active contours," in *Proc. IEEE Conf. Comput. Vis. Pattern Recognit.*, Cambridge, MA, USA, Jun. 1995, pp. 61–79.

[9] R. Malladi, J. A. Sethian, and B. C. Vemuri, "Shape modeling with front propagation: A level set approach," *IEEE Trans. Pattern Anal. Mach. Intell.*, vol. 17, no. 2, pp. 158–175, Mar. 1995.

[10] A. Vasilevskiy and K. Siddiqi, "Flux maximizing geometric flows," *IEEE Trans. Pattern Anal. Mach. Intell.*, vol. 24, no. 12, pp. 1565–1578, Dec. 2002.

[11] C. Li, C. Xu, C. Gui, and M. D. Fox, "Level set evolution without re-initialization: A new variational formulation," in *Proc. IEEE Comput. Soc. Conf. Comput. Vis. Pattern Recognit. (CVPR)*, vol. 1, Jun. 2005, pp. 430–436.

[12] B. Wang, X. Gao, D. Tao, and X. Li, "A nonlinear adaptive level set for image segmentation," *IEEE Trans. Cybern.*, vol. 44, no. 3, pp. 418–428, Mar. 2014.

[13] C. Liu, W. Liu, and W. Xing, "An improved edge-based level set method combining local regional fitting information for noisy image segmentation," *Signal Process.*, vol. 130, pp. 12–21, Jan. 2017.

[14] L. A. Vese and T. F. Chan, "A multiphase level set framework for image segmentation using the Mumford and Shah model," *Int. J. Comput. Vis.*, vol. 50, no. 3, pp. 271–293, Dec. 2002.

[15] J. Lie, M. Lysaker, and X.-C. Tai, "A binary level set model and some applications to mumford-shah image segmentation," *IEEE Trans. Image Process.*, vol. 15, no. 5, pp. 1171–1181, May 2006.

[16] S. Lankton and A. Tannenbaum, "Localizing region-based active contours," *IEEE Trans. Image Process.*, vol. 17, no. 11, pp. 2029–2039, Nov. 2008.

[17] T. Brox and D. Cremers, "On local region models and a statistical interpretation of the piecewise smooth mumford-shah functional," *Int. J. Comput. Vis.*, vol. 84, no. 2, pp. 184–193, Jul. 2008.

[18] X.-F. Wang, H. Min, L. Zou, and Y.-G. Zhang, "A novel level set method for image segmentation by incorporating local statistical analysis and global similarity measurement," *Pattern Recognit.*, vol. 48, no. 1, pp. 189–204, Jan. 2015.

[19] T. F. Chan and L. A. Vese, "Active contour without edges," *IEEE Trans. Image Process.*, vol. 10, no. 2, pp. 266–277, Feb. 2001.

[20] C. Li, C.-Y. Kao, J. C. Gore, and Z. Ding, "Minimization of region-scalable fitting energy for image segmentation," *IEEE Trans. Image Process.*, vol. 17, no. 10, pp. 1940–1949, Oct. 2008.

[21] K. Zhang, H. Song, and L. Zhang, "Active contours driven by local image fitting energy," *Pattern Recognit.*, vol. 43, no. 4, pp. 1199–1206, Apr. 2010.

[22] S. Liu and Y. Peng, "A local region-based Chan–Vese model for image segmentation," *Pattern Recognit.*, vol. 45, no. 7, pp. 2769–2779, Jul. 2012.

[23] S. Niu, Q. Chen, L. de Sisternes, Z. Ji, Z. Zhou, and D. L. Rubin, "Robust noise region-based active contour model via local similarity factor for image segmentation," *Pattern Recognit.*, vol. 61, pp. 104–119, Jan. 2017.

[24] C. R. Meyer, P. H. Bland, and J. Pipe, "Retrospective correction of intensity inhomogeneities in MRI," *IEEE Trans. Med. Imag.*, vol. 14, no. 1, pp. 36–41, Mar. 1995.

[25] Y. Chen, J. Zhang, and J. Yang, "An anisotropic images segmentation and bias correction method," *Magn. Reson. Imag.*, vol. 30, no. 1, pp. 85–95, Jan. 2012.

[26] C. He, Y. Wang, and Q. Chen, "Active contours driven by weighted region-scalable fitting energy based on local entropy," *Signal Process.*, vol. 92, no. 2, pp. 587–600, Feb. 2012.

[27] L. Wang, Y. Chang, H. Wang, Z. Wu, J. Pu, and X. Yang, "An active contour model based on local fitted images for image segmentation," *Inf. Sci.*, vols. 418–419, pp. 61–73, Dec. 2017.

[28] C. Li, R. Huang, Z. Ding, J. C. Gatenby, D. N. Metaxas, and J. C. Gore, "A level set method for image segmentation in the presence of intensity inhomogeneities with application to MRI," *IEEE Trans. Image Process.*, vol. 20, no. 7, pp. 2007–2016, Jul. 2011.

[29] K. Zhang, L. Zhang, K.-M. Lam, and D. Zhang, "A level set approach to image segmentation with intensity inhomogeneity," *IEEE Trans. Cybern.*, vol. 46, no. 2, pp. 546–557, Feb. 2016.

[30] B. Dong, R. Jin, and G. Weng, "Active contour model based on local bias field estimation for image segmentation," *Signal Process., Image Commun.*, vol. 78, pp. 187–199, Oct. 2019.

[31] G. Huang, H. Ji, and W. Zhang, "A fast level set method for inhomogeneous image segmentation with adaptive scale parameter," *Magn. Reson. Imag.*, vol. 52, pp. 33–45, Oct. 2018.

[32] X. Shan, X. Gong, and A. K. Nandi, "Active contour model based on local intensity fitting energy for image segmentation and bias estimation," *IEEE Access*, vol. 6, pp. 49817–49827, 2018.

[33] L. Wang, G. Chen, D. Shi, Y. Chang, S. Chan, J. Pu, and X. Yang, "Active contours driven by edge entropy fitting energy for image segmentation," *Signal Process.*, vol. 149, pp. 27–35, Aug. 2018.

[34] L. Wang, L. Zhang, X. Yang, P. Yi, and H. Chen, "Level set based segmentation using local fitted images and inhomogeneity entropy," *Signal Process.*, vol. 167, Feb. 2020, Art. no. 107297, doi: 10.1016/j.sigpro.2019.107297.

[35] Y. Chen, X. Yue, R. Y. D. Xu, and H. Fujita, "Region scalable active contour model with global constraint," *Knowl.-Based Syst.*, vol. 120, pp. 57–73, Mar. 2017.

[36] Z. Zhang and J. Song, "An adaptive fuzzy level set model with local spatial information for medical image segmentation and bias correction," *IEEE Access*, vol. 7, pp. 27322–27338, 2019.

[37] M. J. Swain and D. H. Ballard, "Color indexing," *Int. J. Comput. Vis.*, vol. 7, no. 1, pp. 11–32, 1991.

XIAOYING SHAN received the B.S. and M.S. degrees from the School of Mathematics and Applied Mathematics, Zhengzhou University, Zhengzhou, China, in 2005 and 2008, respectively. She is currently pursuing the Ph.D. degree with the College of Electronic and Information Engineering, Tongji University, Shanghai, China. Her research interests include medical image processing and computer vision.

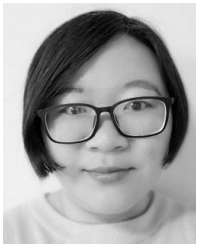

XIAOLIANG GONG received the Ph.D. degree in physics from East China Normal University, in 2012. She is currently an Engineer with the College of Electronic and Information Engineering of Tongji University, Shanghai, China. Her research topics are in biological signal processing, including ECG, EEG, and MRI, and so on.

YINGCHUN REN received the Ph.D. degree from Tongji University, Shanghai, China, in 2017. He is currently a Lecturer with the College of Mathematics Physics and Information Engineering, Jiaxing University, Jiaxing, China. His research interests include pattern recognition, machine learning, and computer vision.

ASOKE K. NANDI (Fellow, IEEE) received the Ph.D. degree from the Trinity College, University of Cambridge, Cambridge, U.K.

He held academic positions in several universities, including Oxford University, U.K., Imperial College London, U.K., the University of Strathclyde, U.K., and the University of Liverpool, U.K. In 2013, he moved to Brunel University London, U.K., as the Chair and the Head of electronic and computer engineering. He was a Finland Distinguished Professor with the University of Jyvaskyla, Jyvaskyla, Finland. He is currently an Adjunct Professor with the University of Calgary, Calgary, Canada. In 1983, he co-discovered of the three fundamental particles known as W^+, W^-, and Z^0 (the UA1 team at CERN), providing the evidence for the unification of the electromagnetic and weak forces, which was recognized by the Nobel Committee for Physics, in 1984. He has made many fundamental theoretical and algorithmic contributions to many aspects of signal processing and machine learning. He has much expertise in big data, dealing with heterogeneous data and extracting information from multiple data sets obtained in different laboratories and different times. He has authored over 600 technical publications, including 240 journal articles as well as five books, entitled *Condition Monitoring with Vibration Signals: Compressive Sampling and Learning Algorithms for Rotating Machines* (Wiley, 2020), *Automatic Modulation Classification: Principles, Algorithms and Applications* (Wiley, 2015), *Integrative Cluster Analysis in Bioinformatics* (Wiley, 2015), *Blind Estimation Using Higher- Order Statistics* (Springer, 1999), and *Automatic Modulation Recognition of Communications Signals* (Springer, 1996). The H-index of his publications is 75 (Google Scholar) and his ERDOS number is two. His current research interests include in the areas of signal processing and machine learning, with applications to communications, image segmentation, and biomedical data.

Prof. Nandi is a Fellow of The Royal Academy of Engineering and seven other institutions. Among the many awards, he received the IEEE (USA) Heinrich Hertz Award, in 2012, the Glory of Bengal Award for his Outstanding Achievements in Scientific Research, in 2010, the Water Arbitration Prize of the Institution of Mechanical Engineers, U.K., in 1999, and the Mountbatten Premium, Division Award of the Electronics and Communications Division, of the Institution of Electrical Engineers, U.K., in 1998. He was an IEEE Distinguished Lecturer of the EMBS Society, from 2018 to 2019.